Persistent opto-ferroelectric responses in molecular ferroelectrics

Xuanyuan Jiang,[1] Xiao Wang,[2] Pratyush Buragohain,[1] Andy T. Clark,[2] Haidong Lu,[1] Shashi Poddar,[1] Le Yu,[2,3] Anthony D. DiChiara,[4] Alexei Gruverman,[1,5] Xuemei Cheng,[2] and Xiaoshan Xu[1,5,*]

[1]*Department of Physics and Astronomy, University of Nebraska, Lincoln, Nebraska 68588, USA*
[2]*Department of Physics, Bryn Mawr College, Bryn Mawr, Pennsylvania 19010, USA*
[3]*School of Electronic Science and Engineering, Nanjing University, Nanjing 210093, China*
[4]*Advanced Photon Source, Argonne National Laboratory, Lemont, Illinois 60439, USA*
[5]*Nebraska Center for Materials and Nanoscience, University of Nebraska, Lincoln, Nebraska 68588, USA*

(Received 7 March 2022; accepted 30 June 2022; published 29 July 2022)

Persistent photoresponses require optical excitations to metastable states, which are rare of ionic origin due to the indirect photon-ion interaction. In this work, we explore the photoinduced metastable proton states in the proton-transfer type molecular ferroelectric croconic acid. We observe that, after the photoexcitation, the changes of structural and ferroelectric properties relax in $\sim 10^3$ s, indicating persistent photoresponses of ionic origin. In contrast, the photoconductivity relaxes within 1 s. The 10^3 s timescale suggests that the ionic metastable states result from proton transfer both along and out of the hydrogen bonds. This discovery unveils an ionic mechanism for the phototunability, which offers persistent opto-ferroelectric control for proton-transfer type molecular ferroelectrics.

DOI: 10.1103/PhysRevMaterials.6.074412

I. INTRODUCTION

The timescale of a material's photoresponses, a key parameter of optical properties, can vary many orders of magnitude. For instance, light reflection and absorption are normally electronic responses that occur in femtoseconds, while the electrons may excite to metastable states leading to persistent responses such as hour-long photoluminescence and photoconductivity [1–4].

Persistent photoresponse hinges on photoexcitation to metastable states. The polarization states in ferroelectric materials offer natural candidates for ionic metastable states. As illustrated in Fig. 1(a), according to the Frank-Condon principle [5–7], photoexcitation mostly starts with electronic excitation in a "vertical" fashion in femtoseconds without changing the vibrational states of the ions. The excited electronic states modify the potential energy landscape of the ions and change the vibrational eigenstates. The ions acquire energy indirectly, in the form of only a few vibrational energy quanta (phonons) by transitioning to the modified states. The probability of photoexcitation to ionic metastable states then depends on the distortion of the ionic potential energy caused by the electronic excited states and the mass of the ions. In this regard, the proton-transfer type molecular ferroelectrics [8–11] is promising given the strong electron-proton coupling and the small mass of proton.

Croconic acid (CA) is a prototypical example of proton-transfer type molecular ferroelectrics, which consists of stacked herringbone layers [12,13], as shown in Fig. 1(b). While these layers are held together by the van der Waals interactions, the molecules within a layer are connected by the (ridge and plane) hydrogen bonds (H bond). As depicted in Fig. 1(c), the protons in the hydrogen bonds have two energy minima resulting from the double-well potentials. CA crystals exhibit spontaneous polarization due to the ordering of proton positions on the same side of the double wells with a Curie temperature higher than 400 K [13]. Recently, CA has demonstrated application potential in ferroelectric control of spintronic devices [14].

Polarization switching of CA corresponds to the collective transfer of protons to the other wells, or transition between two tautomers [12]. The vibrational energy quantum can be estimated as ~0.1 eV using the uncertainty principle for a proton in a well of about 0.5 Å wide, which is comparable to the hydrogen-bond energy [15]. Therefore, the acquisition of a couple of vibrational energy quanta is enough for protons to transfer to the other well as a metastable state. In addition, croconic acid has a large spontaneous polarization ($\approx 20\ \mu C/cm^2$) [12,13] originating from both the ordered protons and the distorted electronic cloud [9,16–18]. The electronic excitation is expected to have a significant impact on the proton potential well [9,19] and promote the protons to the metastable states.

In this work, we studied the responses of structural, ferroelectric, and electric transport properties to photoexcitation in CA films. Reversible changes have been observed in crystal structure and piezoresponse on the order of 10^3 s, indicating dominant ionic contributions.

II. EXPERIMENT

CA films were fabricated by physical vapor deposition in high vacuum (1×10^{-7} Torr) with an EvoVac system from

*xiaoshan.xu@unl.edu

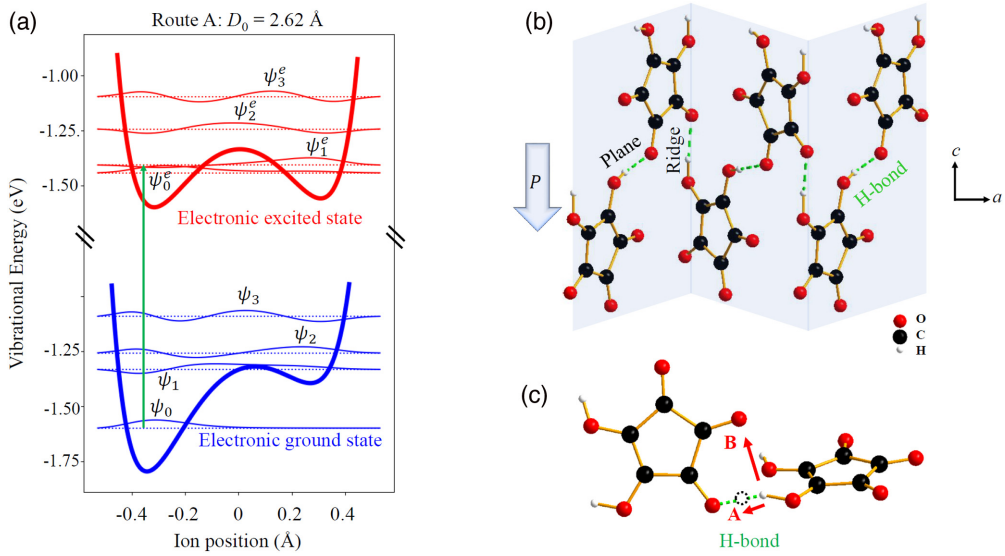

FIG. 1. (a) Simulated potential energy landscapes (thick lines) and the vibrational eigenstates (thin lines) of protons in croconic acid hydrogen bonds. The eigenstates are plotted on the dashed baselines indicating the eigenenergies. The vertical arrow indicates possible proton transfer after the "vertical" electronic excitation. (b) Fragment of a herringbone layer of the croconic acid crystal structure. The spontaneous polarization is pointing down. (c) Two croconic acid molecules connected by a ridge hydrogen bond. The dashed circle indicates the other energy minimum of the proton. The arrows indicate the two potential proton-transfer routes.

Angstrom Engineering on different substrates: 300 nm films on Al_2O_3 substrate for time-resolved x-ray diffraction (XRD), 140 nm films on patterned Au/SiO_2 substrate with 60 nm Al_2O_3 capping layer for photocurrent measurements, and 40 nm films on conductive $NiCo_2O_4/MgAl_2O_4$ for piezoresponse force microscopy (PFM). The time-resolved x-ray diffraction on CA films was carried out at room temperature at beamline 14-ID-B at the Advanced Photon Source in the Argonne National Laboratory [20]. Optical excitation during the x-ray diffraction studies was provided by laser pulses (500 Hz) with 2 μJ/mm^2 (100 mW/cm^2) fluence and 330 nm wavelength (3.8 eV) with an electronically adjustable time delay. The photoconductivity was measured by an impedance analyzer Solartron 1260, with 1 V and 100 Hz with a commercial diode laser with 400 nm wavelength (3.1 eV) with 140 mW/cm^2 fluence. The dimension of the conduction channel is 10 μm × 100 nm × 80 nm. Local PFM spectroscopic studies were carried out using a commercial MFP-3D system from Asylum Research using Cr/Pt/Ir-coated Si probes, in the resonant enhanced mode using a ∼350 kHz AC signal with 0.8 V drive amplitude. The bias was applied to the tip and the bottom electrode was grounded in the PFM measurements. The light source used in the PFM study has 390 nm wavelength (3.2 eV) with 15 mW/cm^2 fluence.

III. RESULTS AND DISCUSSION

A. Photostriction

We studied the photostriction and its timescale of polycrystalline CA films using time-resolved XRD, as demonstrated previously on other ferroelectric materials [20–22]. The experimental setup is depicted in Fig. 2(a). The lattice constants were extracted from the structural refinement using the software FULLPROF based on the $Pca2_1$ crystal structure (Supplemental Material, Figs. S1 and S2) [13,23–26], as shown in Figs. 2(b) and 2(c).

Starting at zero time in Fig. 2(b), the film sample was photoexcited. All lattice constants increase, consistent with the expected positive photostriction, because photoexcitation reduces the order of the protons and molecules which are otherwise tightly packed. At about 300 s (τ_1), while the lattice expansion continues, the rate of lattice expansion reduces; the lower expansion rate remains for a timescale of 10^3 (τ_2). Figure 2(c) displays the lattice change after the photoexcitation is stopped at zero time. The lattice constants decrease slowly until they relax back to approximately the original values before the photoexcitation. Interestingly, there also appears to be two timescales including a fast one (τ_1) and a slow one (τ_2) on the order of 10^2 s and 10^3 s, respectively.

To check the impact of temperature increase (due to the light absorption) to the lattice expansion, we measured the thermal expansion of the CA films directly. As shown in Fig. 2(d), when the CA films were heated, all lattice constants increased compared with the room-temperature values, but with a large anisotropy: The thermal expansion coefficients are 50, 80, and 27 ppm/K along the *a*, *b*, and *c* axes, respectively. The anisotropy of the thermal expansion is consistent with the crystal structural anisotropy of CA [13,25] and previous measurements [27]: the largest expansion is along the *b* axis which is the direction along which the herringbone layers are held together by the van der Waals interaction. The large difference in anisotropy between Fig. 2(b) and Fig. 2(d) suggests that the effect of thermal expansion to the observed photostriction is minimal.

B. Opto-ferroelectric responses

The transfer of protons to the metastable states may also manifest in the ferroelectric properties of the CA films. More

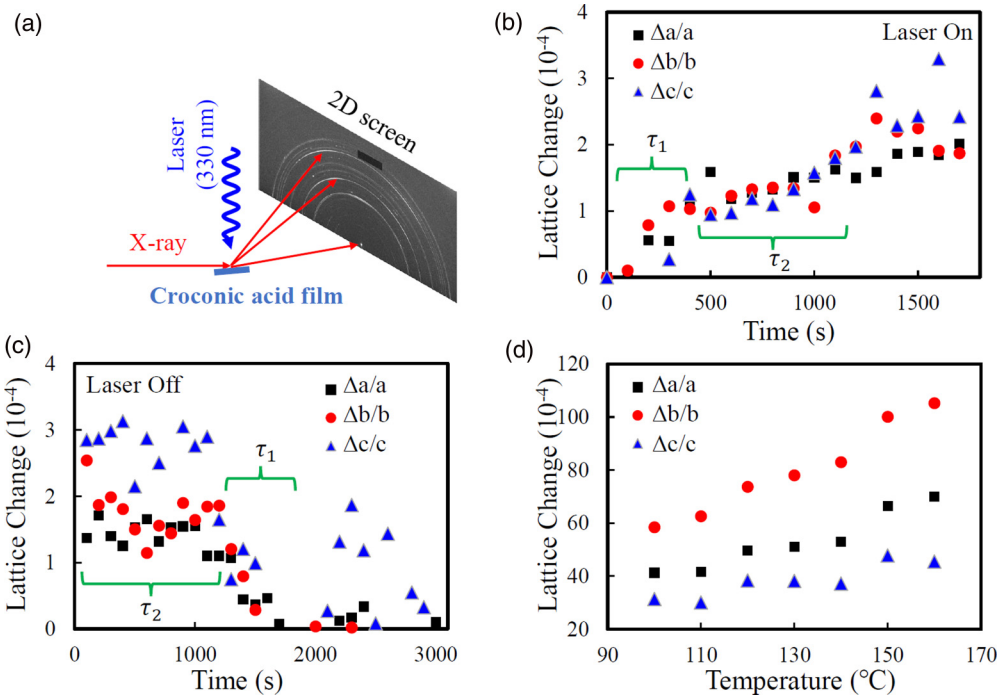

FIG. 2. (a) Experimental setup for time-resolved synchrotron x-ray diffraction. (b) Time-resolved lattice distortion along three axes under photoexcitation starting at zero time. (c) Lattice relaxation after the laser is turned off at zero time. (d) Lattice change due to the thermal expansion with a large anisotropy with respect to the room-temperature values.

specifically, as illustrated in Fig. 1(a), when the protons transfer to the other side of the double well, local dipole moments opposite to the global polarization direction are generated, corresponding to an additional internal field. We studied the ferroelectric switching behavior of the photoexcited CA films using PFM [28–30]. Previously, we demonstrated that continuous CA films consisting of nanometer-sized grains can be prepared on conducting oxide films [31–33] and single-grain ferroelectric switching can be achieved using the conductive tip of a scanning probe as the top electrode [34]. As depicted in Fig. 3(a), using the PFM, the time evolution of piezoresponse of the CA grains was measured. Clear butterfly-type hysteresis loops have been observed, indicative of polarization switchability. The coercive voltage is about 6 V (Supplemental Material, Fig. S3) [26], in agreement with our previous results measured on films grown under similar conditions [35].

Interestingly, the piezoresponse hysteresis loops after photoexcitation, show dramatic asymmetry that is correlated with the initial polarization state [Fig. 3(b)]. The hysteresis loops are shifted to the right immediately after the photoexcitation; correspondingly, the piezoresponses for the positively and negatively poled states at zero bias show large contrasts (>2). The voltage shift of the hysteresis loop in Fig. 3(b) indicates

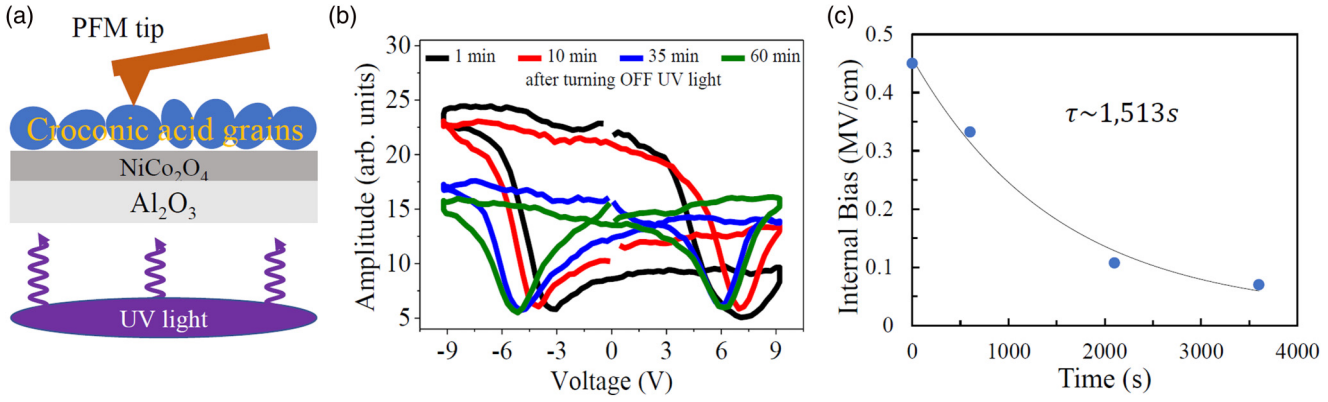

FIG. 3. (a) Schematic diagram of the internal bias study via piezoresponse force microscope (PFM) under the illumination. (b) Hysteretic piezoresponse amplitude at different time after photoexcitation stops, showing shape distortions and shifts of the response along the voltage axis. (c) Internal bias from (b) as a function of relaxation time and the corresponding fit assuming exponential decay. The error bar is 0.01 MV/cm.

the existence of an internal bias field that is opposite to the field generated by the initial polarization. The asymmetry slowly decays over time after the photoexcitation is turned off and the hysteresis loop becomes symmetric after about 1 h. To analyze the time evolution of the asymmetry, we plotted the internal bias as a function of time after the photoexcitation in Fig. 3(c); a fit assuming exponential decay results in a time constant of 1.5×10^3 s, consistent with the timescale of the slow process observed in photostriction.

C. Domainlike and defectlike metastable states

Combining the results from the measurement of photostriction and the measurement of photoinduced changes in piezoresponses, the origin of two metastable states of different timescales may be inferred.

The decay of 10^2 s timescale was observed in photostriction [Fig. 2(c)] but not in the internal bias field in the polarization switching processes [Fig. 3(b)], suggesting that the energy scale of the related metastable state is comparable or less than that of the ferroelectric domain walls. This is consistent with the metastable states resulting from proton transfer along the hydrogen bonds [9,10,19], indicated as route A in Fig. 1(c); the configuration can be viewed as the reversed single-molecule ferroelectric domain. We call this the domainlike metastable state. During the polarization switching process (hysteresis loop measurement), the domainlike metastable state cannot survive because the electric field is expected to wipe out all the domain walls and generate a single domain.

The 10^3 s timescale was observed in both measurements, suggesting a different metastable state. The longer timescale of this metastable state is consistent with a larger energy scale than that of the domain walls since the polarization switching process cannot remove this metastable state. We propose that this metastable state results from proton transfer to another nearby oxygen site, indicated as route B in Fig. 1(c). Also depicted in Fig. 1(c) is the slight bending (155°) of hydrogen bond toward the other oxygen along route B in the crystal structure [35], suggesting sizable attractive force. In this metastable state, with the broken hydrogen bond, the hydrogen becomes an interstitial/vacancy defect. We call this defectlike metastable state. The proton is further away from the originally bonded oxygen site, making it more difficult to return to the ground state, consistent with the internal bias field that cannot be removed by the polarization switching process. Another possible origin for the internal bias is the charge carriers in trap states [36,37], which can be ruled out because our photoconductivity measurements show a < 1 s timescale (Supplemental Material, Fig. S4) [26].

Previous studies using optical second harmonic generation indicated a component of the photoresponses of proton-transfer type ferroelectric crystals up to the microsecond range [9,10]. Calculations found that the lowest excited electronic state of the CA molecules carries a dipole moment opposite to the polarization direction of the CA crystal [9,19]. Based on these findings, simulations assuming adiabatic processes suggest that the photoinduced electronic excitation causes proton transfer to the other side of the hydrogen bonds [9], similar to the route A shown in Fig. 1(c), generating metastable states in the form of local reversed ferroelectric domains. However, the observation of two metastable states, especially one that cannot be removed by the polarization switching process, suggests a more complex process that involves different proton-transfer routes.

D. Double-well model

Here we analyze the proton-transfer process in terms of the response of proton vibrational states to the change of double well after the "vertical" electronic excitation. We employ a double-well model in which most parameters can be estimated using the known CA crystal structure and a hydrogen-bond energy, except for the asymmetry parameter which describes the change of double well due to electronic excitation. The simplicity of the model allows a straightforward illustration of the physical process and comparison between multiple proton-transfer routes.

The potential energy of a proton is assumed to come from two neighboring oxygen sites separated by distance D_0:

$$V_{\mathrm{DW}}(x) = -\frac{a(1-\delta)}{\left(x-\frac{D_0}{2}\right)^4} + \frac{b}{\left(x-\frac{D_0}{2}\right)^8} - \frac{a(1+\delta)}{\left(x+\frac{D_0}{2}\right)^4} + \frac{b}{\left(x+\frac{D_0}{2}\right)^8}, \tag{1}$$

where a and b are parameters for the attractive and repulsive forces of the oxygen sites and δ is the asymmetry parameter. For CA crystals, a and b can be determined using hydrogen-bond energy E_{HB}, proton-oxygen distance x_0, and the hydrogen-bond length L, which are known from the CA crystal structure (Supplemental Material, Figs. S5, S6, and Table S1) [26]. The variable δ describes the change of the double-well potential caused by the electronic excitation. One can numerically solve the vibrational eigenstates by diagonalizing the Hamiltonian [38] with the potential energy $V_{\mathrm{DW}}(x)$.

For the proton transfer along route A (to domainlike metastable states), we use the structural parameters $x_0 = 0.977$ Å, $L = 1.641$ Å, and $D_0 = 2.618$ Å (Supplemental Material, Figs. S5, S6, and Table S1) [26] and assuming $E_{\mathrm{HB}} = 0.3$ eV [15,39]. The asymmetry parameters are assumed to be $\delta_g = 0.1$ and $\delta_e = 0.01$ with the electronic ground state and the electronic excited state, respectively.

As shown in Fig. 1(a), with the electronic ground state, a significant asymmetry is introduced to the proton potential well using $\delta_g = 0.1$, due to the local field generated by the spontaneous polarization. The energy barrier in the middle is consistent with the result from the previous first-principles calculations [9]. The proton (vibrational) ground state ψ_0 is local in the left well with an energy lower than the barrier. The ~0.1 eV separation between the ψ_0 and ψ_1 is consistent with the estimated vibrational energy quantum from the uncertainty principle, which suggests the protons stay mostly in the ground state ψ_0.

With the electronic excited state, a corresponding dipole moment [9,19] generates a field opposite to the local field and reduces the asymmetry of the double well. We represent the

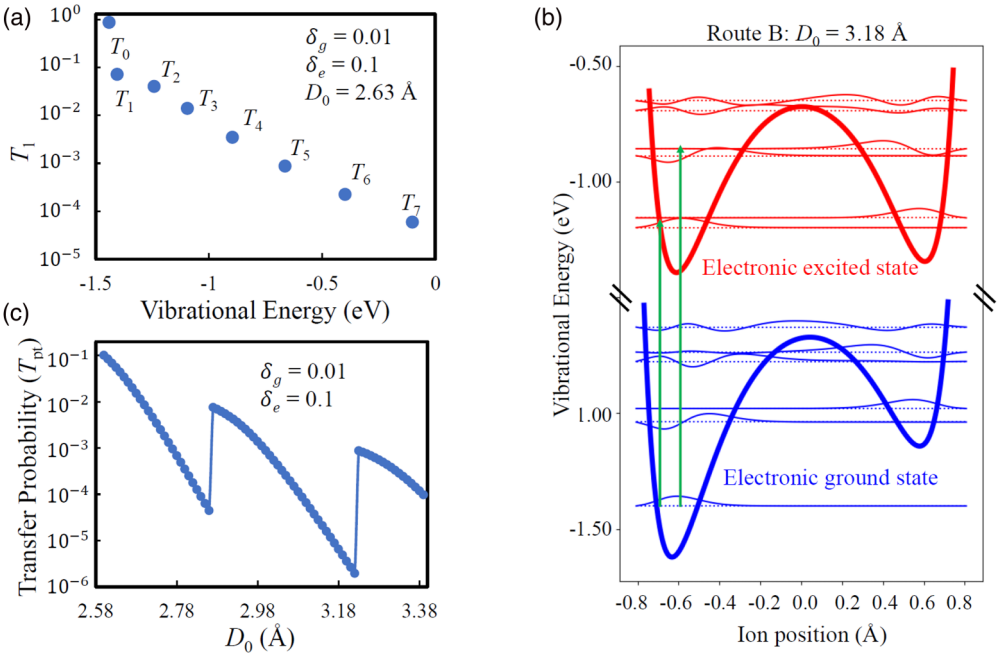

FIG. 4. (a) Transition probability from the vibrational ground state to the modified eigenstates due to the change of potential energy landscape. (b) Simulated potential energy landscapes (thick lines) and the vibrational eigenstates (thin lines) of protons. The eigenstates are plotted on the dashed baselines indicating the eigenenergies. The vertical arrows indicate the potential proton transfer after the "vertical" electronic excitation. (c) The proton transfer probability as a function of oxygen-oxygen site distance.

effect using a smaller value $\delta_e = 0.01$ for the proton potential. The two local states, ψ_0^e and ψ_1^e, due to the reduced asymmetry, change substantially from ψ_0 and ψ_1, respectively, suggesting a sizable probability for the proton to transfer from ψ_0 (left well) to ψ_1^e (right well). Figure 4(a) displays the transition probability $T_n = |\langle\psi_n^e|\psi_0\rangle|^2$ as a function of the vibrational energy of the ψ_n^e state. The probability drops quickly with energy because the higher energy states are less affected by the asymmetry change of the well and tend to remain orthogonal to ψ_0. Therefore, the proton can only acquire efficiently a few vibrational energy quanta.

The change of asymmetry from δ_g to δ_e is critical for the proton transfer. The total probability of proton transfer from the left well to the right well is $T_{pt} = \sum T_i = \sum |\langle\psi_i^e|\psi_0\rangle|^2$ for all ψ_i^e states localized in the right well. It can be shown (Supplemental Material, Fig. S7) [26], when $\delta_e/\delta_g \to 1$, i.e., toward no change of asymmetry, $T_{\rm pt}$ drops quickly. In contrast, $T_{\rm pt}$ is much less sensitive to δ_g alone if δ_e/δ_g is constant. Notice that δ is a parameter in the model that is hard to estimate from the known data of CA crystals. The insensitivity of $T_{\rm pt}$ to δ_g makes the model more valid.

For the proton transfer along route B (to defectlike metastable states), we use $D_0 = 3.18$ Å in the model (Supplemental Material, Figs. S5, S6, and Table S1) [26], with other parameters kept the same. The results are displayed in Fig. 4(b). As the two wells are more separated, the states are more localized compared with those in Fig. 1(a). In addition, larger D_0 also makes the barrier between the two wells higher for there is less attraction from the other oxygen site. As a result, additional local states appear. Figure 4(c) shows the calculated $T_{\rm pt}$ as a function of D_0. In general, larger D_0 reduces $T_{\rm pt}$ due to the localization of the vibrational states. On the other hand, when additional local states appear, $T_{\rm pt}$ get boosted, which is the case for route B ($D_0 = 3.18$ Å). This could be a mechanism for protons to follow route B to reach the defectlike metastable state.

Overall, the double-well model offers plausible mechanisms for the two proton metastable states that lead to two different timescales of the photoresponses, with two key factors: (1) a significant change of protons double-well symmetry due to the electronic excitation, i.e., strong electron-proton coupling [9,16–18] and (2) few local vibrational eigenstates so that the change of double-well symmetry can efficiently modify these states. These factors are not expected in traditional oxide ferroelectrics. As a result, the ionic photoresponses of materials like $PbTiO_3$ are dominated by the classical converse piezoelectric effects following the electronic excitation in the form of photovoltaic effect with a nanosecond timescale [21,40], or simply thermal expansion [20].

IV. CONCLUSION

We have demonstrated persistent ($\sim 10^3$ s) reversible structural responses to photoexcitation in croconic acid using time-resolved x-ray diffraction. The effect correlates with the buildup of the internal electric field which relaxes in a similar timescale, while the photoconductivity decays within 1 s. These observations indicate that photoexcitation can effectively promote protons to metastable states, which in turn have long-lasting impacts on material properties. In particular, for proton-transfer type ferroelectrics, this mechanism generates persistent opto-ferroelectric effects which offers novel control of ferroelectricity and the related devices such as multiferroic tunnel junctions [14]. The gradual and persistent

photoresponses are also promising for emulating the photocontrolled plasticity for neuromorphic computing applications.

ACKNOWLEDGMENTS

This research was primarily supported by the U.S. Department of Energy (DOE), Office of Science, Basic Energy Sciences, under Award No. DE-SC0019173 (device fabrication, transport measurements, x-ray diffraction, and modeling). Additional support was from the National Science Foundation (NSF) under Grant No. DMR-1420645 (PFM). Work at Bryn Mawr College was supported by NSF Grant No. DMR-1708790. This research used resources of the Advanced Photon Source, a U.S. DOE Office of Science User Facility operated for the DOE Office of Science by Argonne National Laboratory under Contract No. DE-AC02-06CH11357. Use of BioCARS was also supported by the National Institute of General Medical Sciences of the National Institutes of Health (NIH) under Grant No. R24GM111072. The content is solely the responsibility of the authors and does not necessarily represent the official views of the NIH. Time-resolved setup at Sector 14 was funded in part through a collaboration with Philip Anfinrud (NIH/National Institute of Diabetes and Digestive and Kidney Diseases). The research was performed in part in the Nebraska Nanoscale Facility: National Nanotechnology Coordinated Infrastructure and the Nebraska Center for Materials and Nanoscience (and/or NERCF), which are supported by the NSF under award ECCS: 2025298, and the Nebraska Research Initiative.

[1] T. Matsuzawa, Y. Aoki, N. Takeuchi, and Y. Murayama, A new long phosphorescent phosphor with high brightness, $SrAl_2O_4$: Eu^{2+}, Dy^{3+}, J. Electrochem. Soc. **143**, 2670 (1996).

[2] M. C. Tarun, F. A. Selim, and M. D. McCluskey, Persistent Photoconductivity in Strontium Titanate, Phys. Rev. Lett. **111**, 187403 (2013).

[3] H. Yin, A. Akey, and R. Jaramillo, Large and persistent photoconductivity due to hole-hole correlation in CdS, Phys. Rev. Materials **2**, 084602 (2018).

[4] R. Kabe and C. Adachi, Organic long persistent luminescence, Nature (London) **550**, 384 (2017).

[5] E. Condon, A theory of intensity distribution in band systems, Phys. Rev. **28**, 1182 (1926).

[6] E. U. Condon, Nuclear motions associated with electron transitions in diatomic molecules, Phys. Rev. **32**, 858 (1928).

[7] J. Franck and E. G. Dymond, Elementary processes of photochemical reactions, Trans. Faraday Soc. **21**, 536 (1926).

[8] S. Horiuchi, R. Kumai, and Y. Tokura, Hydrogen-bonding molecular chains for high-temperature ferroelectricity, Adv. Mater. **23**, 2098 (2011).

[9] K. Iwano, Y. Shimoi, T. Miyamoto, D. Hata, M. Sotome, N. Kida, S. Horiuchi, and H. Okamoto, Ultrafast Photoinduced Electric-Polarization Switching in a Hydrogen-Bonded Ferroelectric Crystal, Phys. Rev. Lett. **118**, 107404 (2017).

[10] T. Umanodan, S. I. I. Tanaka, S. Naruse, T. Ishikawa, K. Onda, S. Y. Koshihara, S. Horiuchi, and Y. Okimoto, Different time-scale relaxation dynamics in organic supramolecular ferroelectrics studied by linear and nonlinear spectroscopy, J. Phys. Soc. Jpn. **84**, 073707 (2015).

[11] Y. Y. Tang, J. C. Liu, Y. L. Zeng, H. Peng, X. Q. Huang, M. J. Yang, and R. G. Xiong, Optical control of polarization switching in a single-component organic ferroelectric crystal, J. Am. Chem. Soc. **143**, 13816 (2021).

[12] S. Horiuchi, K. Kobayashi, R. Kumai, and S. Ishibashi, Proton tautomerism for strong polarization switching, Nat. Commun. **8**, 14426 (2017).

[13] S. Horiuchi, Y. Tokunaga, G. Giovannetti, S. Picozzi, H. Itoh, R. Shimano, R. Kumai, and Y. Tokura, Above-room-temperature ferroelectricity in a single-component molecular crystal, Nature (London) **463**, 789 (2010).

[14] Y. Yin, Y. Yin, X. Jiang, M. A. Koten, J. E. Shield, X. Chen, Y. Yun, A. T. N'Diaye, X. Hong, and X. Xu, Spin Rectification and Electrically Controlled Spin Transport in Molecular-Ferroelectrics-Based Spin Valves, Phys. Rev. Appl. **13**, 064011 (2020).

[15] K. Wendler, J. Thar, S. Zahn, and B. Kirchner, Estimating the hydrogen bond energy, J. Phys. Chem. A **114**, 9529 (2010).

[16] F. Tang, X. Jiang, H. Y. Ko, J. Xu, M. Topsakal, G. Hao, A. T. N'Diaye, P. A. Dowben, D. Lu, X. Xu, and X. Wu, Probing ferroelectricity by x-ray absorption spectroscopy in molecular crystals, Phys. Rev. Materials **4**, 034401 (2020).

[17] Y. Cai, S. Luo, Z. Zhu, and H. Gu, Ferroelectric mechanism of croconic acid: A first-principles and Monte Carlo study, J. Chem. Phys. **139**, 044702 (2013).

[18] J. Seliger, J. Plavec, P. Šket, V. Žagar, and R. Blinc, ^{17}O NQR and ^{13}C NMR study of hydrogen-bonded organic ferroelectric croconic acid, Physica Status Solidi B **248**, 2091 (2011).

[19] T. Miyamoto, D. Hata, T. Morimoto, H. Yamakawa, N. Kida, T. Terashige, K. Iwano, H. Kishida, S. Horiuchi, and H. Okamoto, Ultrafast polarization control by terahertz fields via π-electron wavefunction changes in hydrogen-bonded molecular ferroelectrics, Sci. Rep. **8**, 15014 (2018).

[20] K. Sinha, Y. Zhang, X. Jiang, H. Wang, X. Wang, X. Zhang, P. J. Ryan, J. W. Kim, J. Bowlan, D. A. Yarotski *et al.*, Effects of biaxial strain on the improper multiferroicity in $h-LuFeO_3$ films studied using the restrained thermal expansion method, Phys. Rev. B **95**, 094110 (2017).

[21] D. Daranciang, M. J. Highland, H. Wen, S. M. Young, N. C. Brandt, H. Y. Hwang, M. Vattilana, M. Nicoul, F. Quirin, J. Goodfellow *et al.*, Ultrafast Photovoltaic Response in Ferroelectric Nanolayers, Phys. Rev. Lett. **108**, 087601 (2012).

[22] H. Wen, P. Chen, M. P. Cosgriff, D. A. Walko, J. H. Lee, C. Adamo, R. D. Schaller, J. F. Ihlefeld, E. M. Dufresne, D. G. Schlom *et al.*, Electronic Origin of Ultrafast Photoinduced Strain in $BiFeO_3$, Phys. Rev. Lett. **110**, 037601 (2013).

[23] F. Bisti, A. Stroppa, F. Perrozzi, M. Donarelli, S. Picozzi, M. Coreno, M. de Simone, K. C. Prince, and L. Ottaviano, The electronic structure of gas phase croconic acid compared to the condensed phase: More insight into the hydrogen bond interaction, J. Chem. Phys. **138**, 014308 (2013).

[24] F. Bisti, A. Stroppa, S. Picozzi, and L. Ottaviano, Fingerprints of the hydrogen bond in the photoemission spectra of croconic acid condensed phase: An x-ray photoelectron spectroscopy and *ab-initio* study, J. Chem. Phys. **134**, 174505 (2011).

[25] D. di Sante, A. Stroppa, and S. Picozzi, Structural, electronic and ferroelectric properties of croconic acid crystal: A DFT study, Phys. Chem. Chem. Phys. **14**, 14673 (2012).

[26] See Supplemental Material at http://link.aps.org/supplemental/10.1103/PhysRevMaterials.6.074412 for more details on structural analysis, opto-ferroelectric and photoconductivity characterizations, and theoretical modeling.

[27] S. Mukhopadhyay, M. Gutmann, and F. Fernandez-Alonso, Hydrogen-bond structure and anharmonicity in croconic acid, Phys. Chem. Chem. Phys. **16**, 26234 (2014).

[28] A. Gruverman, O. Auciello, and H. Tokumoto, Imaging and control of domain structures in ferroelectric thin films via scanning force microscopy, Annu. Rev. Mater. Sci. **28**, 101 (1998).

[29] A. Gruverman, M. Alexe, and D. Meier, Piezoresponse force microscopy and nanoferroic phenomena, Nat. Comm. **10**, 1661 (2019).

[30] D. A. Bonnell, S. v. Kalinin, A. L. Kholkin, and A. Gruverman, Piezoresponse force microscopy: A window into electromechanical behavior at the nanoscale, MRS Bull. **34**, 648 (2009).

[31] Y. Yuan, X. Jiang, S. Poddar, and X. Xu, Electric-field assisted nucleation processes of croconic acid films, CrystEngComm **21**, 7460 (2019).

[32] C. Zhen, X. Zhang, W. Wei, W. Guo, A. Pant, X. Xu, J. Shen, L. Ma, and D. Hou, Nanostructural origin of semiconductivity and large magnetoresistance in epitaxial $NiCo_2O_4/Al_2O_3$ thin films, J. Phys. D Appl. Phys. **51**, 145308 (2018).

[33] C. Mellinger, J. Waybright, X. Zhang, C. Schmidt, and X. Xu, Perpendicular magnetic anisotropy in conducting $NiCo_2O_4$ films from spin-lattice coupling, Phys. Rev. B **101**, 014413 (2020).

[34] X. Jiang, H. Lu, Y. Yin, X. Zhang, X. Wang, L. Yu, Z. Ahmadi, P. S. Costa, A. D. DiChiara, X. Cheng *et al.*, Room temperature ferroelectricity in continuous croconic acid thin films, Appl. Phys. Lett. **109**, 102902 (2016).

[35] D. Braga, L. Maini, and F. Grepioni, Crystallization from hydrochloric acid affords the solid-state structure of croconic acid (175 years after its discovery) and a novel hydrogen-bonded network, CrystEngComm **3**, 27 (2001).

[36] D. Dimos, W. L. Warren, M. B. Sinclair, B. A. Tuttle, and R. W. Schwartz, Photoinduced hysteresis changes and optical storage in (Pb, La)(Zr, Ti)O_3 thin films and ceramics, J. Appl. Phys. **76**, 4305 (1994).

[37] R. H. Bube and S. A. Rice, *Photoconductivity of Solids* (Wiley, New York, 1960).

[38] F. Marsiglio, The harmonic oscillator in quantum mechanics: A third way, Am. J. Phys. **77**, 253 (2009).

[39] F. Fernandez-Alonso, M. J. Gutmann, S. Mukhopadhyay, D. B. Jochym, K. Refson, M. Jura, M. Krzystyniak, M. Jiménez-Ruiz, and A. Wagner, Hydrogen bonding in the organic ferroelectric croconic acid: Insights from experiment and first-principles modelling, J. Phys. Soc. Jpn. **82**, SA001 (2013).

[40] S. Matzen, L. Guillemot, T. Maroutian, S. K. K. Patel, H. Wen, A. D. DiChiara, G. Agnus, O. G. Shpyrko, E. E. Fullerton, D. Ravelosona *et al.*, Tuning ultrafast photoinduced strain in ferroelectric-based devices, Adv. Electron. Mater. **5**, 1800709 (2019).